Photoselected electron transfer pathways in DNA photolyase

Tatiana R. Prytkova[†], David N. Beratan[†‡], and Spiros S. Skourtis[‡§]

[†]Departments of Chemistry and Biochemistry, Duke University, Durham, NC 27708; and [§]Department of Physics, University of Cyprus, P.O. Box 20537, Nicosia 1678, Cyprus

Edited by Joshua Jortner, Tel Aviv University, Tel Aviv, Israel, and approved November 13, 2006 (received for review June 27, 2006)

Cyclobutane dimer photolyases are proteins that bind to UV-damaged DNA containing cyclobutane pyrimidine dimer lesions. They repair these lesions by photo-induced electron transfer. The electron donor cofactor of a photolyase is a two-electron-reduced flavin adenine dinucleotide ($FADH^-$). When $FADH^-$ is photo-excited, it transfers an electron from an excited $\pi \rightarrow \pi^*$ singlet state to the pyrimidine dimer lesion of DNA. We compute the lowest excited singlet states of $FADH^-$ using ab initio (time-dependent density functional theory and time-dependent Hartree–Fock), and semiempirical (INDO/S configuration interaction) methods. The calculations show that the two lowest $\pi \rightarrow \pi^*$ singlet states of $FADH^-$ are localized on the side of the flavin ring that is proximal to the dimer lesion of DNA. For the lowest-energy donor excited state of $FADH^-$, we compute the conformationally averaged electronic coupling to acceptor states of the thymine dimer. The coupling calculations are performed at the INDO/S level, on donor–acceptor cofactor conformations obtained from molecular dynamics simulations of the solvated protein with a thymine dimer docked in its active site. These calculations demonstrate that the localization of the $^1FADH^{-*}$ donor state on the flavin ring enhances the electronic coupling between the flavin and the dimer by permitting shorter electron-transfer pathways to the dimer that have single through-space jumps. Therefore, in photolyase, the photo-excitation itself enhances the electron transfer rate by moving the electron towards the dimer.

Cyclobutane pyrimidine dimer (CPD) photolyases bind to CPD lesions of UV-damaged DNA and repair them by photo-induced electron transfer (ET) (see refs. 1–3 for reviews). The electron donor cofactor of a photolyase is a two-electron-reduced flavin adenine dinucleotide ($FADH^-$). $FADH^-$ transfers an electron to the protein-bound CPD lesion of DNA upon photo-excitation with 350- to 450-nm light. This ET step initiates the cleavage of the dimer bonds and the repair of the lesion (conversion to two pyrimidine monomers). $FADH^-$ can be excited either directly by absorption of a photon, or indirectly from the chromophore cofactor of photolyase. The latter acts as an antenna molecule, absorbing light and transferring its energy to $FADH^-$ via dipole–dipole interactions. The chromophore is either methenyltetrahydrofolate in folate class photolyases or 8-hydroxy-7,8-didemethyl-deazariboflavin (8-HDF) in deazaflavin class photolyases.

Structures of both folate and deazaflavin class photolyases are known from x-ray crystallography (4–6). Only the most recent structure is a complex between the photolyase and DNA (a DNA oligomer that contains a cyclobutane thymine dimer analog; ref. 6). The protein is bound to the DNA oligomer at the location of the dimer lesion, and the dimer lies inside the protein's active site [a binding mode also suggested by biochemical, fluorescence, and NMR experiments (1–3, 7–9), and investigated in several computational studies (10–14)]. In the active site, the dimer is adjacent to $FADH^-$ (6). The C4 carbonyl groups of the dimer's 5′-T and 3′-T form hydrogen bonds with the amino N6 of the adenine portion of $FADH^-$. Furthermore, the C4 carbonyl in 3′-T is adjacent to the C8 methyl group of the flavin moiety of $FADH^-$ (4 Å) (Fig. 1*a*).

The ET reaction that initiates dimer repair, $^1FADH^{-*}$ +Pyr-Pyr $\xrightarrow{e^-}$ $FADH^\bullet$ + Pyr-$Pyr^{\bullet -}$, involves the transfer of an electron from an excited singlet $\pi \rightarrow \pi^*$ state of $FADH^-$, at a rate of the order of 100^{-1} $psec^{-1}$. Stuchebrukhov and coworkers (13, 14) performed detailed analysis of this ET reaction mechanism. Using docking and molecular dynamics simulations, they predicted the location of the dimer relative to $FADH^-$ that was later observed in the crystal structure (6). They also calculated the electronic structure of the donor and acceptor states of the $FADH^-$–dimer system, and the donor–acceptor electronic coupling, using the extended-Hückel method and tunneling current analysis (15). They predicted that ET takes place by a tunneling mechanism that does not involve protein (non-$FADH^-$) intermediates. The experimental evidence supports this mechanism (see refs. 1–3 for reviews).

In refs. 13 and 14, the $\pi \rightarrow \pi^*$ electron donor state of $FADH^{-*}$ was taken to be the (extended-Hückel) lowest occupied molecular orbital (LUMO) of the flavin ring. This LUMO has most of its electron amplitude localized on atoms C4, O4, and C10, i.e., on the side of the ring that is furthest away from the dimer (hereby denoted the distal side, Fig. 1*a*). For this donor state, the computed rms tunneling matrix element is on the order of 10^{-3} eV. Furthermore, tunneling current calculations showed that the main ET path to the dimer begins in the C4, C10, N10 region of flavin, continues with a through-space jump to the adenine ring (from C1′–H of flavin to C6–N6 of adenine), and ends with a second through space jump from the adenine to the dimer (N6 of the adenine ring to the C4 carbonyl groups of 5′-T and 3′-T in the dimer) (13, 14). Therefore, the adenine ring is described as acting as a superexchange bridge between the distal side of the flavin moiety of $FADH^-$ and the dimer lesion (13, 14).

Here, we reexamine the subject of the donor-state localization on the flavin ring, and we investigate how this localization influences the flavin–dimer electronic coupling and the ET pathways. We first compute the lowest excited singlet states of $FADH^-$ using *ab initio* [time-dependent Hartree–Fock (TDHF) (16) and time-dependent density functional theory (TDDFT) (17, 18)], and semiempirical (INDO/S configuration interaction; refs. 19 and 20) methods. The calculations show that the lowest $\pi \rightarrow \pi^*$ singlet states of $FADH^-$ that are localized on the flavin moiety have most of their amplitude on the benzene side of the flavin ring, adjacent to the dimer (hereby denoted the proximal side, Fig. 1*a*). To analyze the electronic coupling between $FADH^-$ and the dimer, we compute the conformationally averaged tunneling matrix elements between empty dimer orbitals and the donor state of $FADH^-$ (the lowest $\pi \rightarrow \pi^*$ singlet state). The coupling calculations are performed at the

Author contributions: T.R.P., D.N.B., and S.S.S. designed research; T.R.P. and S.S.S. performed research; T.R.P. and S.S.S. contributed new reagents/analytic tools; T.R.P., D.N.B., and S.S.S. analyzed data; and T.R.P., D.N.B., and S.S.S. wrote the paper.

The authors declare no conflict of interest.

This article is a PNAS direct submission.

Abbreviations: TDHF, time-dependent Hartree-Fock; TDDFT, time-dependent density functional theory; CIS, configuration interaction singles; ET, electron transfer.

[‡]To whom correspondence may be addressed. E-mail: david.beratan@duke.edu or skourtis@ucy.ac.cy.

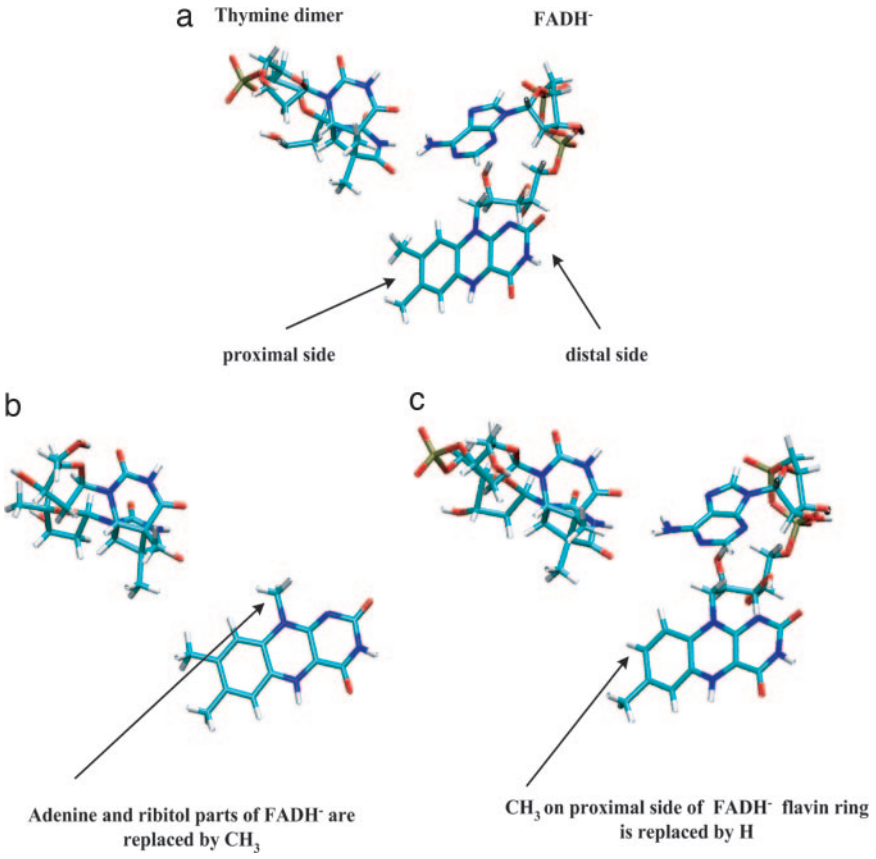

Fig. 1. Diagram showing donor and acceptor molecular structures. (*a*) Pyrimidine dimer–$FADH^-$ geometry taken from an MD snapshot of solvated *E. coli* photolyase with a thymine dimer docked in the active side. (*b*) The modified flavin cofactor obtained by deleting the ribytol and adenine moieties of $FADH^-$ and replacing them by a methyl group at the C1′ position. (*c*) The modified flavin cofactor obtained by deleting the C8 methyl group on the proximal side of the flavin ring with a hydrogen.

INDO/S level using MD simulations of the protein with a thymine dimer docked in its active site.

To explore the structure of the ET pathways between the donor and the dimer acceptor states, we also perform tunneling matrix element calculations using modified flavin cofactors as donor molecules, constructed by pruning $FADH^-$. The modifications of $FADH^-$ are performed in such a way so as to erase either adenine mediated ET pathways (that always contain at least two through-space jumps) or the more direct C8-methyl mediated pathways (that contain one through-space jump). In one kind of structure modification, the ribytol and adenine moieties of $FADH^-$ are deleted and replaced by a methyl group at the C1′ position (Fig. 1*b*). These deletions eliminate all ET pathways through the adenine ring. In the other kind of modification, we replace the C8 methyl group on the proximal side of the flavin ring with a hydrogen (Fig. 1*c*). The hydrogen atoms of the C8 methyl group are close to the C4 carbonyl of 3′-T of the dimer (Fig. 1*a*). Therefore, their deletion diminishes the strength of the direct ET pathways between the flavin and the dimer that contain single through space jumps.

We find that the above chemical modifications of $FADH^-$ do not appreciably change the character and relative energies of the lowest $\pi \rightarrow \pi^*$ singlet states of the flavin ring. Therefore, we use the same type of electron donor state for the modified cofactors as we did for the full $FADH^-$ (i.e., the lowest singlet $\pi \rightarrow \pi^*$ state of the flavin ring localized on its proximal side). Furthermore, the conformational averaging of the tunneling matrix elements for the modified cofactors is performed using MD snapshots created as follows. For each snapshot of the $FADH^-$–dimer subsystem obtained from the original protein–dimer simulations, we delete the $FADH^-$ atoms and perform the atom replacements described above (Fig. 1) without perturbing the positions of the remaining $FADH^-$ atoms, nor the conformation of the adjacent dimer. Therefore, the conformationally averaged matrix elements with the flavin cofactor of Fig. 1*b* used as the donor are computed using dimer–flavin ring trajectories that are identical to the dimer–ring trajectories of the original simulations. A similar approach is used for the other cofactor (Fig. 1*c*), in which case the MD trajectories used to compute matrix element averages differ from the full $FADH^-$–dimer trajectories only for four atoms (the C8 methyl group). For $FADH^-$ and the modified flavin cofactors, we analyze the magnitudes of the donor–acceptor coupling fluctuations in terms of the coherence parameter (21–24).

Results and Discussion

Excited-State Electronic Structure Calculations. The aim of the excited-state calculations is to identify the lowest $\pi \rightarrow \pi^*$ singlet state of $FADH^-$, which we take to be the electron–donor state for the ET reaction: $^1FADH^{-*}$ + Pyr-Pyr $\xrightarrow{e^-}$ $FADH^\bullet$ + $Pyr\text{-}Pyr^{\bullet -}$. Because of the large size of $FADH^-$ and the need to calculate its excited states in different geometries, it is practical to use single-reference quantum-chemical methods (25, 26). These include TD-DFT, TDHF theory, and semiempirical methods (such as INDO/S configuration interaction singles, CIS). To gauge the reliability of our calculations, we used all of these methods and sought robust predictions. We performed the electronic-structure calculations on several molecular geometries derived from different protein–$FADH^-$–dimer MD conformations. Furthermore, each calculation was performed in the solvation environment of the protein's active site (including active site residues, water, and the thymine dimer), whose total charge was varied.

In the 300- to 500-nm range, the observed absorption spectrum of *Escherichia coli* photolyase with only the $FADH^-$ cofactor (no methenyltetrahydrofolate chromophore; ref. 1) has a maximum of $\varepsilon \approx 3 \times 10^4$ (M^{-1} cm^{-1}) at $\lambda = 300$ nm, dropping to a minimum value of $\varepsilon_{min} \approx 5 \times 10^3$ (M^{-1} cm^{-1}) at $\lambda_{min} \approx 340$ nm. For longer wavelengths, the absorption spectrum has a secondary maximum of $\varepsilon_{max} \approx 6$–$7 \times 10^3$ (M^{-1} cm^{-1}) at $\lambda_{max} \approx 365$ nm. Absorption vanishes as λ approaches 500 nm. Because we are only interested

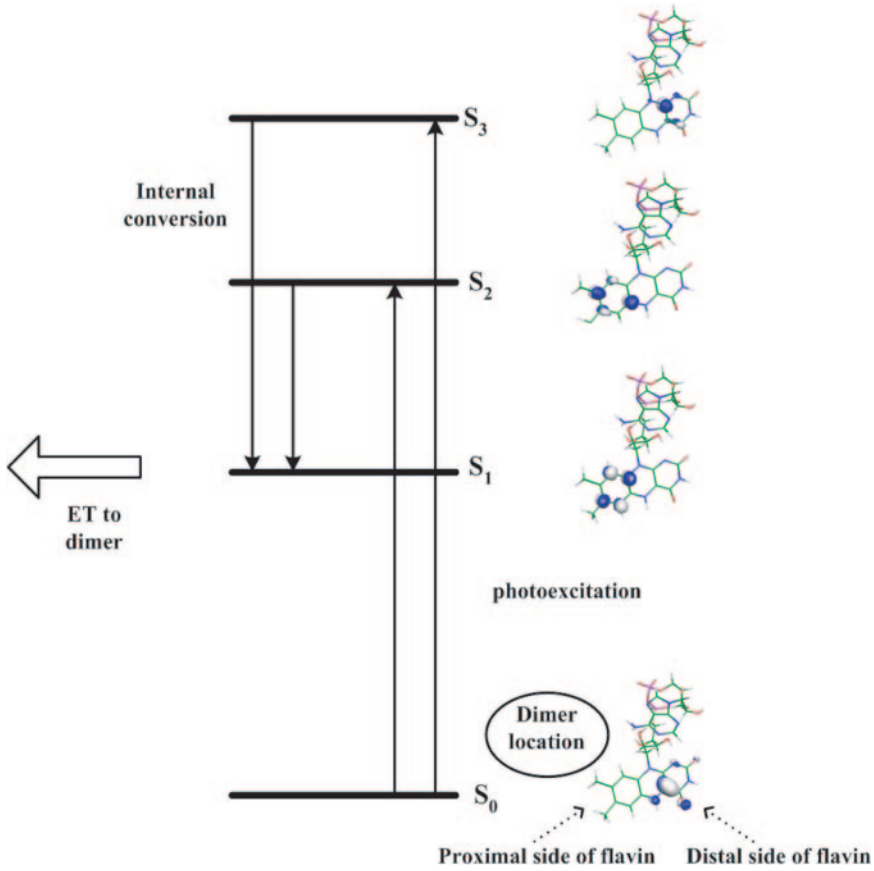

Fig. 2. Diagram showing photo-excitation of the $^1FADH^-$ ground state to the $^1FADH^-$* S_2 and S_3 excited states. Relaxation to the lowest $^1FADH^-$* S_1 excited state is followed by ET to the dimer.

in the lowest singlet excited state of $FADH^-$, the relevant region of the spectrum for our calculations is the low-maximum region centered at $\lambda_{max} \approx 365$ nm.

The INDO/S calculations predict that the two lowest singlet excited states of $FADH^-$ (S_1 and S_2 of Fig. 2) are of $\pi \rightarrow \pi^*$ character, and they involve the displacement of electron amplitude from the distal side to the proximal side of the flavin ring. S_1 and S_2 have dipole moments 12.9 D and 13.1 D relative to ground state, respectively. At higher energies, there is also a $\pi \rightarrow \pi^*$ singlet excited state (S_3 in Fig. 2) that retains the electron amplitude on the distal side of the flavin ring (with dipole moment of 1.6 D relative to the ground state), and $\pi \rightarrow \pi^*$ states that displace electron amplitude from the distal side of the flavin ring to the adenine ring. S_1 has negligible oscillator strength and cannot be related to the experimental absorption spectrum. S_2 has observable oscillator strength and an absorption wavelength slightly beyond the low maximum of the experimental spectrum (predicted $f = 2–3 \times 10^{-1}$, $\lambda = 390–400$ nm). S_3 has the highest oscillator strength and absorption wavelength smaller than $\lambda_{min} \approx 340$ nm (predicted $f = 4.0–4.5 \times 10^{-1}$, $\lambda = 320–330$ nm). The flavin to adenine $\pi \rightarrow \pi^*$ states have negligible oscillator strengths. The ranges of the reported wavelength and oscillator-strength values reflect different results from the MD snapshots and the total solvation charges that were tested. The INDO/S calculations allow us to identify the low maximum in the experimental absorption spectrum with the S_2 excited state, because the predicted wavelengths for S_2 are the closest to the experimental $\lambda_{max} \approx 365$ nm among the S_n wavelengths. Importantly, the INDO/S oscillator strength of S_2 for the majority of the $FADH^-$ MD conformations ($f = 0.2$) corresponds to $\varepsilon \approx 6 \times 10^3$ (M^{-1} cm^{-1}), which is approximately the experimental value of $\varepsilon_{max} \approx 6–7 \times 10^3$ (M^{-1} cm^{-1}).

The TDDFT/BHandHLYP calculations compute the 10 lowest singlet excited states of $FADH^-$. They predict flavin-flavin $\pi \rightarrow \pi^*$ excitations that are similar to the INDO/S S_1 and S_2, and low-lying flavin-adenine $\pi \rightarrow \pi^*$ excitations (the S_3 type state lies beyond the energy range of the 10 lowest singlets). For S_1 and S_2, the TDDFT wavelengths are slightly smaller (by 10–20 nm) than the INDO/S values. The oscillator strength for S_2 is of the order of 10^{-1} (as in INDO/S), and the strengths for S_1 and the flavin–adenine excitations are negligible. TDHF greatly underestimates the absorption wavelengths (this is a known shortcoming of the method; ref. 25).

In conclusion, Fig. 2 summarizes the state scheme for the lowest flavin–flavin $\pi \rightarrow \pi^*$ excitations of solvated $FADH^-$ that emerges from the semiempirical and *ab initio* TDDFT calculations, and is consistent with the experimental absorption spectrum of $FADH^-$ in photolyase. This scheme is also consistent with early semiempirical analysis of flavin spectra and with flavin spectroscopic data (refs. 27–29 and references therein). The excitations shown in Fig. 2 are properties of the flavin moiety of $FADH^-$, and they are not determined by the solvation environment of the protein active site (we observe the same state ordering and electron localization for the modified cofactors of Fig. 1 *b* and *c*, and for $FADH^-$ in vacuum).

Upon photo-excitation, we expect that the high-oscillator-strength S_2 and S_3 states will be populated, with S_3 having greater population than S_2. The rate of the photo-induced ET reaction is $\approx 200^{-1}$ $psec^{-1}$ (30). For excited states with highly overlapping vibrational levels, (as in the flavin-localized excited states), the time scale of $S_n \rightarrow S_1$ relaxation is of the order of 1 psec or less. There is evidence from time-resolved absorption and fluorescence experiments on flavin compounds (31, 32) that the internal conversion rate in the π^* singlet excited state manifold is a few hundred

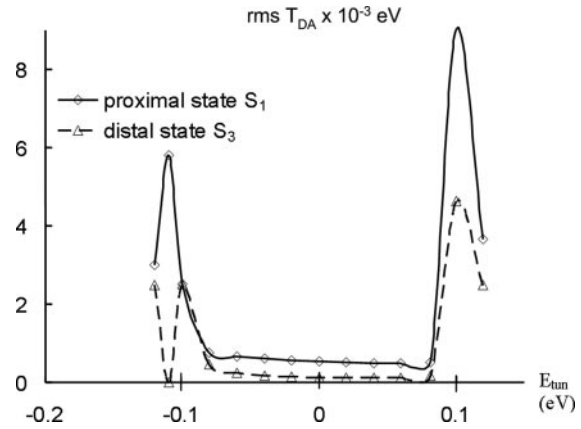

Fig. 3. The tunneling energy dependence of $T_{DA}^{(rms)} = \sqrt{\langle T_{DA}^2 \rangle}$ for two different choices of donor state: the excited MO of S_1 (proximal side of flavin), and the excited MO of S_3 (distal side of flavin), both shown in Fig. 2.

femtoseconds to 1 psec. Therefore, before ET, we expect that the donor excited state has relaxed to S_1 and is localized on the proximal side of the flavin ring, adjacent to the dimer.

The observation in our calculations of low-lying flavin–adenine $\pi \rightarrow \pi^*$ singlet excited states raises the question of whether the donor electron density may be localized on the adenine ring before the ET reaction to the dimer. Because the oscillator strength of these states are very low compared to S_2 and S_3, we do not expect appreciable population of the adenine ring upon photo-excitation. Adenine can only be populated if it accepts the excited electron from the flavin (i.e., through a resonant tunneling or hopping mechanism) before ET from $FADH^-$ to the dimer. Recent femtosecond time-resolved spectroscopy of the ET reaction $^1FADH^{-*}$ + Pyr-Pyr $\xrightarrow{e^-}$ $FADH^\bullet$ + Pyr-$Pyr^{\bullet -}$ in *E. coli* photolyase has excluded this possibility (30). There is no observation of ET to adenine in that experiment, even in the absence of the dimer. The absence of a real adenine intermediate supports the prediction of Stuchebrukhov and coworkers (13, 14) that ET takes place by a single superexchange step.

Tunneling Matrix Element Calculations. Having concluded that the electron donor state for the photo-induced ET reaction is localized on the proximal side of the flavin ring, we now explore how this state couples to the dimer electron-accepting orbitals. The donor–acceptor electronic coupling may arise from the tunneling matrix element between the donor state and any empty thymine dimer state that becomes nearly resonant with the donor state.

As mentioned in the Introduction, we examined three donor cofactors (the full $FADH^-$ molecule and the modified cofactors of Fig. 1). For each cofactor, and for the different donor molecular orbital (MO)–acceptor MO pairs, we computed the conformational averages $\langle T_{DA} \rangle$ and $\langle T_{DA}^2 \rangle$, using dimer-$FADH^-$ MD snapshots from the MD simulations of photolyase with the thymine dimer docked in its active site. The computations of the tunneling matrix element were performed at the INDO/S level, and were based on Green's function (33) and energy splitting methods (34). In all computations with the Green's function approach, we examined the tunneling energy dependence of our results.

Fig. 3 is derived from a thymine dimer–full $FADH^-$ calculation, where we show the tunneling-energy dependence of $T_{DA}^{(rms)} = \sqrt{\langle T_{DA}^2 \rangle}$ for two different choices of the donor state: first, the excited MO of S_1 (proximal side of the flavin) and second, the excited-MO of S_3 (distal side of flavin) (see Fig. 2). Although we propose that S_1 is the actual donor for the ET reaction $^1FADH^{-*}$ + Pyr-Pyr $\xrightarrow{e^-}$ $FADH^\bullet$ + Pyr-$Pyr^{\bullet -}$, we use both MOs as donors in order to probe the tunneling-energy dependence of the coupling and to locate bridge resonances. T_{DA} is calculated with the Green's function method and the conformational averages of the coupling are computed from 100 MD snapshots separated by 1-psec time intervals. Furthermore, for each donor MO, the plotted $T_{DA}^{(rms)}$ values are averages of four $T_{DA}^{(rms)}$ values involving different acceptor MOs. The four acceptor MOs are empty orbitals of the thymine dimer that are closest in energy to the donor orbital. The solid line in the plot refers to the S_1 donor and the dotted line to S_3. For a wide range of tunneling energies, each $T_{DA}^{(rms)}$ remains approximately constant. Sharp changes in $T_{DA}^{(rms)}$ are observed only around $E_{tun} \approx \pm 0.1$ eV, but these E_{tun} regions are not physically relevant because the D and A MO energies in the MD simulations fluctuate within the flat region of the plot [the sharp increase in $T_{DA}^{(rms)}$ at $E_{tun} \approx \pm 0.1$ eV indicates that these E_{tun} values are near-resonant with bridge electronic states]. The flat behavior of $T_{DA}^{(rms)}$ in the physically relevant energy range, regardless of the localization of the donor state on the flavin, is consistent with a tunneling mechanism for the ET step from the flavin to the dimer. Fig. 3 also shows that $T_{DA}^{(rms)}$ for the proximal D state (S_1) is about four times greater than $T_{DA}^{(rms)}$ for the distal D state (S_3) for all tunneling energies in the physical range. This difference in $T_{DA}^{(rms)}$ magnitudes reflects the different localizations of the S_1 and S_3 states with respect to the thymine dimer.

Table 1. rms T_{DA} and coherence parameter for the dimer with full $FADH^-$ (Fig. 1*a*)

E_{tun}, eV	$T_{DA}^{(rms)}$, eV	R_{coh}
0.08	5.11×10^{-4}	0.075
0.06	4.78×10^{-4}	0.056
0.04	4.83×10^{-4}	0.049

$T_{DA}^{(rms)} = \sqrt{\langle T_{DA}^2 \rangle}$ and $R_{coh} = \langle T_{DA} \rangle^2 / \langle T_{DA}^2 \rangle$ for the thymine dimer–$FADH^-$ pair (Fig. 1*a*) as a function of tunneling energy (Green's function method). $T_{DA}^{(rms)}$ computed with the energy splitting method is 2.76×10^{-4} eV.

We now analyze the electronic coupling pathways between the proposed donor state for the photo-induced ET reaction (S_1 of Fig. 2) and the thymine dimer acceptor states. The semiempirical and *ab initio* calculations described above showed that there are low-energy adenine-localized virtual MOs that could act as superexchange bridge orbitals that couple the donor and the acceptor states. We investigate this possibility by comparing the electronic couplings computed using the full $FADH^-$ molecule (Fig. 1*a*) to the couplings computed using the modified cofactors shown in Fig. 1 *b* and *c*.

Table 1 shows $T_{DA}^{(rms)}$ and the coherence parameter $R_{coh} = \langle T_{DA} \rangle^2 / \langle T_{DA}^2 \rangle$ values for the thymine dimer–full $FADH^-$ cofactor pair (R_{coh} measures the magnitude of the coupling fluctuations compared to the average coupling; ref. 21). The values of $T_{DA}^{(rms)}$ and R_{coh} shown in the table are averages over four D–A MO pairs where the D MO is the π^* orbital of S_1 (Fig. 2), and the A MOs are empty orbitals of the thymine dimer that are closest in energy to D. T_{DA} is computed using the Green's function method with E_{tun} equal to 0.04, 0.06, and 0.08 eV. These values of E_{tun} correspond approximately to the average energies of the D–A pairs mentioned above, and they are located in the flat region of Fig. 3. The $T_{DA}^{(rms)}$ and R_{coh} averages were computed using 100 MD snapshots separated by 1 psec time intervals (similar values for $T_{DA}^{(rms)}$ were obtained by averaging over 100 MD snapshots separated by 1 fsec time intervals). The results in Table 1 show that the rms tunneling matrix element between the proximal D state and the thymine dimer is of the order 5×10^{-4} eV. Further, the coherence parameter is less than 0.1, indicating large fluctuations of the tunneling matrix element with respect to structural changes (i.e., $\sigma_{T_{DA}} \gg \langle T_{DA} \rangle$).

Tables 2 and 3 show $T_{DA}^{(rms)}$ and R_{coh} for the thymine dimer with the modified flavin cofactors of Fig. 1 *b* and *c*, respectively. The D

Table 2. rms T_{DA} and coherence parameter for the dimer with the cofactor of Fig. 1*b*

E_{tun}, eV	$T_{DA}^{(rms)}$, eV	R_{coh}
0.08	5.16×10^{-4}	0.07
0.06	5.48×10^{-4}	0.03
0.04	5.74×10^{-4}	0.04

$T_{DA}^{(rms)} = \sqrt{\langle T_{DA}^2 \rangle}$ and R_{coh} for the system of Fig. 1*b* (Green's function method). $T_{DA}^{(rms)}$ computed with the energy splitting method is 2.5×10^{-4} eV.

Table 3. rms T_{DA} and coherence parameter for the dimer with the cofactor of Fig. 1*c*

E_{tun}, eV	$T_{DA}^{(rms)}$, eV	R_{coh}
0.08	1.28×10^{-4}	0.09
0.06	1.13×10^{-4}	0.03
0.04	1.15×10^{-4}	0.03

$T_{DA}^{(rms)}$ and R_{coh} for the system of Fig. 1*c* (Green's function method). $T_{DA}^{(rms)}$ computed with the energy splitting method is 8.93×10^{-5} eV.

orbitals used in these calculations are very similar to S_1 in Fig. 2, (the calculations are based on the Green's function method). A comparison of $T_{DA}^{(rms)}$ for the thymine dimer–FADH$^-$ system (Table 1) to $T_{DA}^{(rms)}$ for the thymine dimer-modified flavin cofactor systems (Tables 2 and 3) shows that the tunneling matrix element for the proximal donor state is not much affected by the deletion of the adenine-mediated pathways (Table 2). It is, however, reduced by a factor of 4–5 by the deletion of the methyl-mediated pathways (Table 3). These observations indicate that the electronic coupling between the proximal donor state of FADH$^-$ and the dimer acceptor states is mediated mostly by the C8 methyl group that is on the proximal side of the flavin ring, next to the dimer. The proximity of the excited donor state to the C8 methyl group results in the adenine moiety not being an essential mediator of the donor–acceptor electronic coupling.

The three systems in Tables 1–3 have essentially the same donor–acceptor MO pairs and average donor–acceptor distances but different ET pathways and electronic couplings. Their coherence parameters $R_{coh} = \langle T_{DA} \rangle^2 / \langle T_{DA}^2 \rangle$ are very small (<0.1). If we increase the donor–acceptor distance by changing the nature of the donor state (by choosing as D the excited MO of S_3 in Fig. 2), the ET pathways change and $T_{DA}^{(rms)}$ is reduced. However R_{coh} remains the same order of magnitude as before. The small value of the coherence parameter in these systems indicates large fluctuations in the donor–acceptor electronic coupling with geometry. In all cases considered, both the donor state and the thymine acceptor state are delocalized over several atoms that are "connected" by through space interactions. This geometry gives rise to multiple rapidly fluctuating pathways that can interference destructively and constructively depending on subtle aspects of the molecular conformation. The changing interference patterns caused by molecular motion lead to large fluctuations in the tunneling matrix element. The small R_{coh} values observed for FADH$^-$–dimer ET in photolyase are similar to those reported for solvent-mediated ET reactions in small C-clamped molecules (22), for ET in azurin (23), and for the BPh $\rightarrow$ Q_A ET reaction in the bacterial photosynthetic reaction center (24). The common feature of these different ET systems is the existence of multiple destructively interfering pathways that include through space and hydrogen bond couplings.

Conclusions

We have used molecular dynamics simulations and electronic structure analysis to show that the excited donor state associated with the ET reaction ^{1}FADH^{-*} + Pyr-Pyr $\xrightarrow{e-}$ FADH$^\bullet$ + Pyr-Pyr$^{\bullet -}$ in *E. coli* DNA photolyase is localized on the side of the FADH$^-$ flavin ring proximal to the pyrimidine dimer. The localization of the donor excited state enhances the donor–acceptor coupling and the direct through-space ET pathways between FADH$^-$ and the dimer. Our calculations indicate that the donor–acceptor coupling is of the order of 5×10^{-4} eV. If we assume that the ET reaction is activationless (14, 15) with a reorganization energy of $\approx$1 eV, the predicted room temperature ET rate is 230^{-1} psec^{-1}. This value is close to the experimental rate of $(170 \text{ psec})^{-1}$ for ET to a thymine dimer lesion (in *E. coli* photolyase; ref. 30). It should be noted, however, that it is difficult to estimate the reorganization energy of the reaction because there is substantial solvent reorganization of the active site upon photo-excitation (30).

The donor state used here is assumed to be the lowest-energy $\pi \rightarrow \pi^*$ singlet localized on the flavin ring of FADH$^-$ (as experiment excludes localization on adenine; ref. 30). Higher $\pi \rightarrow \pi^*$ singlet states that are populated upon photo-excitation are expected to relax rapidly to this state. The lowest flavin $\pi \rightarrow \pi^*$ singlet of FADH$^-$ involves a large displacement of electron density across the flavin ring, from the pyrimidine to the benzene ring side adjacent to the docked thymine dimer. This type of transition is consistent with the experimental absorption spectrum of *E. coli* photolyase, and it is a property of the flavin ring that is not altered by the protein environment surrounding FADH$^-$. The electron-density displacement upon photo-excitation creates a large dipole moment that should cause substantial solvent reorganization of the active site. Recent time-resolved experiments have observed such photo-induced solvent reorganization (30).

For the proposed donor state, we performed ET pathway analysis on a large number of MD conformations to see whether the adenine moiety of FADH$^-$ acts as a virtual intermediate for the ET step. We found that the adenine is not essential to tunneling because an electron of the excited state on the benzene side of the ring can tunnel to the dimer through the adjacent C8-methyl group that is in direct through-space contact with the dimer. It is difficult, however, to completely rule out superexchange contribution from adenine, because low-probability conformational fluctuations may provide secondary superexchange pathways through this moiety. We believe that a more important role for the adenine moiety in FADH$^-$ is to stabilize the observed dimer–FADH$^-$ conformation sterically inside the active site, and to anchor the dimer to FADH$^-$ by forming adenine–dimer hydrogen bonds (6, 30). This stabilized conformation places the dimer next to the benzene side of the flavin ring. Therefore, the protein can utilize the electron displacement characteristic of the lowest flavin $\pi \rightarrow \pi^*$ transition to direct the electron towards the dimer and to enhance the donor–acceptor coupling.

Computational Methods

MD Simulations. The MD simulations were performed on *E. coli* photolyase (Protein Data Bank ID code 1DNP; ref. 4). The initial conformation of the docked thymine dimer in the protein active site was obtained from refs. 13 and 14. In all MD simulations, we used the Amber 8.0 program (35, 36) and the AMBER force field (37). The dimer and FADH$^-$ partial charges were calculated at the Hartree–Fock level using Gaussian 98 (38) and a 6–31 G(d) basis set. Partial charges were fitted using the RESP procedure (39–41). For FADH$^-$ and the thymine dimer Amber force-field potential types were assigned in the same manner as in refs. 10 and 11. The MD was performed with a constant pressure (NpT) ensemble, Langevin thermostat, periodic boundary conditions, and full electrostatics particle mesh Ewald calculation (42). The structure was solvated with a TIP3P water box of dimensions $95 \times 75 \times 75$ A. Na^+ ions were added to neutralize the system. Crystallographic water molecules within 5 Å of FADH$^-$ were retained. After initial energy minimization of 5,000 steps, with harmonic constraints imposed on

the protein backbone and on the $FADH^-$ and dimer heavy atoms, we followed with 300-psec MD using the same harmonic constraints. The structure was then equilibrated for 500 psec at 300 K without constraints. After the equilibration procedure, MD was performed for 100 psec. During the production run, the relative positions of $FADH^-$ and the dimer were stable, and the rmsd fluctuations were within 1 Å. Conformational snapshots were saved every 1 psec.

Excited-State Electronic Structure Calculations. $FADH^-$ contains π-electrons in regions of space that are spatially separated, i.e., at the opposite sides of the flavin ring (distal and proximal sides in Fig. 1*a*), and in the adenine moiety. Therefore, some of its $\pi \rightarrow \pi^*$ excitations may contain charge transfer (CT) character. Generally, for CT excitations of extended π-systems, single-reference *ab initio* methods can be inaccurate (e.g., refs. 25, 26, and 43–45). In many cases, a semiempirical method parameterized for excited states, such as INDO/S CIS, may be a dependable approach for the computation of the energy spectrum in a large molecule (e.g., refs. 43 and 44). To gauge the reliability of our calculations, we used all of the methods above, INDO/S CIS, TDDFT, and TDHF, and sought robust predictions.

For $FADH^-$, we performed the electronic structure calculations on several molecular geometries derived from different protein–$FADH^-$–dimer MD conformations (separated by 20–80 psec). Each calculation was performed both in vacuum and in the solvation environment of the protein's active site (represented by Amber force-field atomic charges). The solvation environment included the active site residues 222, 234–239, 271, 338, 341, 344, 372, 374, and 378 of *E. coli* photolyase, the thymine dimer, 47 water molecules, and Na^+ ions used for charge neutralization in MD. The Na^+ ions were used in the electronic structure calculations to vary the total charge of the system so that $FADH^-$ is either fully neutralized (total charge 0), or it has an effective charge of -1 (total charge -1). Finally, to probe the effect of the adenine moiety on the $\pi \rightarrow \pi^*$ excitations of $FADH^-$ that are localized on the flavin ring, we also performed the *ab initio* and semiempirical calculations on the modified flavin cofactor of Fig. 1*b* that does not contain the ribytol and adenine moieties. For the INDO/S CIS calculations, we used the program of ref. 46, and for the *ab initio* calculations, we used the program Gaussian03 (47). The dipole moments of the $FADH^-$ ground state and of the singlet excited states denoted S_1, S_2, and S_3 were calculated using the program of ref. 46.

The TDDFT and TDHF calculations computed the 10 lowest singlet excited states of $FADH^-$ using the 6–31+G(d) basis set. Compared to the B3LYP functional (48, 49), the BHandHLYP functional (50) gave the most dependable results, predicting absorption wavelengths close to the INDO/S values that were robust with respect to changes in molecular size (i.e., $FADH^-$ versus the flavin cofactor of Fig. 1*b*).

Tunneling Matrix Element Calculations. The electronic-coupling calculations were performed at the INDO/S level using the Harlem program (51) and two different computational approaches. In one approach (the "Green's function method"), the tunneling matrix element between the donor MO (D) and the acceptor MO (A) is $T_{DA}(E_{tun}) = \{E_{tun}\tilde{S} - \tilde{G}(E_{tun})^{-1}\}_{D,A}$, where $\tilde{G}$ ($\tilde{S}$) is the Green's function (overlap) matrix for the entire donor–acceptor cofactor system, and E_{tun} is the tunneling energy (33). In the other approach (the "energy splitting method"), the donor and acceptor MOs are brought into resonance by application of an external electric field $\bar{E}$ along the donor–acceptor axis (34). The eigenvalues/vectors of the Hamiltonian are computed as a function of the electric-field strength in order to identify minimum energy splittings between eigenvalues (at resonances between coupled MOs). T_{DA} is taken as half the minimum energy splitting created by the resonance of the eigenstates that originate from the initial donor and acceptor MOs. We also performed exploratory INDO/S calculations of T_{DA} for several snapshot geometries using the generalized Mulliken–Hush (GMH) approach (52). This analysis indicates that the electronic couplings calculated with the Green's function method and the GMH method are very similar.

We thank Prof. A. Stuchebrukhov for providing initial structures of photolyase with a thymine dimer docked in its active site, Prof. J.R. Reimers for providing his INDO/S code, and Profs. G. Archontis, I. Kurnikov, J. Reimers, and A. Stuchebrukhov, and Drs. S. Keinan and G. Zuber for stimulating and helpful discussions. S.S.S. acknowledges support from the University of Cyprus research grant "Repair of UV Damaged DNA by DNA Photolyase: Insights from Molecular Dynamics and Electron Transfer Calculations." D.N. Beratan thanks the National Institutes of Health (GM-048043) and the Duke Center for Computational Science, Engineering, and Medicine (CSEM).

1. Sancar A (2003) *Chem Rev* 103:2203–2237.
2. Byrdin M, Sartor V, Eker APM, Vos MH, Aubert C, Brettel K, Mathis P (2004) *Biochim Biophys Acta* 1655:64–70.
3. Weber S (2005) *Biochim Biophys Acta* 1707:1–23.
4. Park H-W, Kim S-T, Sancar A, Deisenhofer J (1995) *Science* 268:1866–1872.
5. Tamada T, Kitadokoro K, Higuchi Y, Inaka K, Yasui A, de Ruiter PE, Eker APM, Miki K (1997) *Nat Struct Biol* 4:887–891.
6. Mees A, Klar T, Gnau P, Hennecke U, Eker APM, Carell T, Essen L-O (2004) *Science* 306:1789–1793.
7. Christine KS, MacFarlane AW, IV, Yang K, Stanley RJ (1998) *J Biol Chem* 277:38339–38344.
8. Vande Berg BJ, Sancar GB (1998) *J Biol Chem* 273:20276–20284.
9. Torizawa T, Ueda T, Kuramitsu S, Hitomi K, Todo T, Iwai S, Morikawa K, Shimada I (2004) *J Biol Chem* 279:32950–32956.
10. Hahn J, Michel-Beyerle M-E, Rösch N (1998) *J Mol Model* 4:73–82.
11. Hahn J, Michel-Beyerle M-E, Rösch N (1999) *J Phys Chem B* 103:2001–2007.
12. Sanders DB, Wiest O (1999) *J Am Chem Soc* 121:5127–5234.
13. Antony J, Medvedev DM, Stuchebrukhov AA (2000) *J Am Chem Soc* 122:1057–1065.
14. Medvedev D, Stuchebrukhov AA (2001) *J Theor Biol* 122:237–248.
15. Stuchebrukhov AA (1996) *J Chem Phys* 194:8424–8432.
16. Dirac PAM (1930) *Proc Cambridge Philos Soc* 26:376–385.
17. Runge E, Gross EKU (1984) *Phys Rev Lett* 52:997–1000.
18. Casida ME, Jamorski C, Casida KC, Salahub DR (1998) *J Chem Phys* 108:4439–4449.
19. Bacon AD, Zerner MC (1979) *Theor Chim Acta* 53:21–54.
20. Zerner MC, Loew GH, Kirchner RF, Mueller-Westerhoff UT (1980) *J Am Chem Soc* 102:589–599.
21. Balabin IA, Onuchic JN (2000) *Science* 290:114–117.
22. Troisi A, Ratner MA, Zimmt MB (2004) *J Am Chem Soc* 126:2215–2224.
23. Skourtis SS, Balabin IA, Kawatsu T, Beratan DN (2005) *Proc Natl Acad Sci USA* 102:3552–3557.
24. Nishioka H, Kimura A, Yamato T, Kawatsu T, Kakitani T (2005) *J Phys Chem B* 109:15621–15635.
25. Drew A, Head-Gordon M (2005) *Chem Rev* 105:4009–4037.
26. Grimme S (2004) in *Reviews in Computational Chemistry*, eds Lipkowitz B, Larter R, Cundary TR (Wiley, New York), Vol 20, pp 153–218.
27. Song P-S (1968) *Int J Quant Chem* II:463–470.
28. Heelis PF (1997) *J Photochem Photobiol B* 38:31–34.
29. Stanley RJ (2001) *Antioxidants Redox Signaling* 3:847–866.
30. Kao Y-T, Saxena C, Wang L, Sancar A, Zhong D (2005) *Proc Natl Acad Sci USA* 102:16128–16132.
31. Enescu M, Lindqvist L, Soep B (1998) *Photochem Photobiol* 68:150–156.
32. Gauden M, Yeremenko S, Lann W, van Stokkum IHM, Ihalainen JA, van Grondelle R, Hellingwerf KJ, Kennis JTM (2005) *Biochemistry* 44:3653–3661.
33. Kurnikov IV, Beratan DN (1996) *J Chem Phys* 105:9561–9573.
34. Prytkova TR, Kurnikov IV, Beratan DN (2005) *J Phys Chem B* 109:1618–1625.
35. Case DA, Darden TA, Cheatham TE, III, Simmerling CL, Wang J, Duke RE, Luo R, Merz KM, Wang B, Pearlman DA, *et al.* (2004) *AMBER 8* (Univ of California, San Francisco).
36. Case DA, Cheatham TE, III, Darden T, Gohlke H, Luo R, Merz KM Jr, Onufriev A, Simmerling C, Wang B, Woods RJ (2005) *J Comput Chem* 26:1668–1688.
37. Ponder JW, Case DA (2003) *Adv Prot Chem* 66:27–85.
38. Frisch MJ, Trucks GW, Schlegel HB, Scuseria GE, Robb MA, Cheeseman JR, Zakrzewski VG, Montgomery JA, Jr, Stratmann RE, Burant JC, *et al.* (2001) Gaussian 98 (Gaussian, Inc, Pittsburgh), Revision A.11.3.
39. Besler BH, Merz KM, Jr, Kollman PA (1990) *J Comput Chem* 11:431–439.
40. Singh UC, Kollman PA (1984) *J Comp Chem* 5:129–145.
41. Bayly CI, Cieplak P, Cornell W, Kollman PA (1993) *J Phys Chem* 97:10269–10280.
42. Essmann U, Perera L, Berkowitz ML, Darden T, Lee H, Pedersen LG (1995) *J Chem Phys* 103:8577–8593.
43. Cai Z-L, Sendt K, Reimers JR (2002) *J Chem Phys* 117:5543–5549.
44. Reimers JR, Cai Z-L, Bilic A, Hush NS (2003) *Ann NY Acad Sci* 1006:235–251.
45. Grimme S, Parc M (2003) *Chem Phys Chem* 3:292–295.
46. Zeng J, Hush NS, Reimers JR (1996) *J Am Chem Soc* 118:2059–2068.
47. Frisch MJ, Trucks GW, Schlegel HB, Scuseria GE, Robb MA, Cheeseman JR, Montgomery Jr JA, Vreven T, Kudin KN, Burant JC, *et al.* (2004) Gaussian 03 (Gaussian, Inc, Wallingford CT), Revision B05.
48. Becke AD (1993) *J Chem Phys* 98:5648–5652.
49. Lee C, Yang W, Parr RG (1998) *Phys Rev B* 37:785–789.
50. Becke AD (1993) *J Chem Phys* 98:1372–1377.
51. Kurnikov IV (2005) HARLEM Molecular Modeling Package (Univ of Pittsburgh, Pittsburgh).
52. Cave RJ, Newton MD (1996) *Chem Phys Lett* 249:15–19.